공학석사학위논문

정지 비행시 날갯짓 비행체의 날개형상에대한 실험적 최적화 연구

An Experimental Optimization of Flapping Wing Geometry in the Hover

2018 년 8 월

서울대학교 대학원

기계항공공학부

Adhikari Dibya Raj

정지 비행시 날갯짓 비행체의 날개형상에대한 실험적 최적화 연구

An Experimental Optimization of Flapping Wing Geometry in the Hover

지도교수 김 종 암

이 논문을 공학석사 학위논문으로 제출함

2018 년 8 월

서울대학교 대학원

기계항공공학부

Adhikari Dibya Raj

Adhikari Dibya Raj 의 공학석사 학위논문을 인준함

2018 년 8 월

위 원 장 _____

부위원장 _____

위 원 _____

Abstract

An Experimental Optimization of Flapping Wing Geometry in the Hover

Adhikari Dibya Raj

Department of Mechanical and Aerospace Engineering

The Graduate School

Seoul National University

Flapping wing of flying insects is a source of motivation for the development of the Flapping Wing Micro Air Vehicles (FWMAV), which can perform both the hover and forward flight with high maneuverability. An efficient design of FWMAV demands the meticulous analysis of the wing design space to obtain the best blend of wing parameters. In this research, we implemented a surrogate based experimental optimization process to enhance the flapping wing performance in the hover flight.

In nature, different insects have distinct combination of wing geometric parameters and these insects produces different degree of aerodynamic performance. To understand the consequences of varying the wing parameters on the flapping wing performance, we first investigate the effect of wing geometric parameters on the mean thrust and power efficiency using the iterative approach. The results show that wing geometric parameters like camber angle, non-dimensional radius of second moment of area and Aspect Ratio have a significant effect on the mean thrust generation and power efficiency. Then, to obtain an optimum wing design, we implemented a surrogate based experimental design optimization process. To consider the noise in the experimental data, a surrogate is constructed using a noisy Kriging model. The objective of this optimization process is to maximize the power efficiency. A new design point, with camber angle of 9.5678^0, non-dimensional radius of second moment of area of 0.5876 and aspect ratio of 8.2925, obtained from this optimization process produced the maximum power efficiency than any other wings. At 26.67 Hz of flapping frequency, this wing generates 20.89 gf of thrust force. The flight capability of this optimized wing is verified by using a wired flight with stabilizer.

Keywords: Flapping wing, Flapping Wing Micro Air Vehicles (FMAVs), hover flight, aspect ratio, camber angle, non-dimensional radius, parametric study, experimental optimization, Kriging model

Student Number: 2016-23334

Contents

List of Figures

List of Tables

Chapter 1

Introduction

1.1 Background

Insect's flight has fascinated several researchers around the world with their agile flight and high maneuverability. Insects produce the lift and thrust forces by flapping their wings. The flapping wing is also responsible for the flight maneuvers. Insect flapping wings can perform both the forward and hover flight and is the proven solution for the Micro Air Vehicles (MAV). Because of the tiny size and their ability to do search and rescue mission, MAVs are of great value to military and civilization application. Although the findings on unsteady aerodynamic [1-3]revoked a well-known myth about the insect's flight, insects cannot fly according to classical aerodynamic theory, little work has been done to produce an optimum flapping wing design for an efficient flight of the flapping wing Micro Air Vehicles (FWMAV).

Over the past few decades, many works have been done on the FWMAVs. However, most of the previous studies are on flapping

wing kinematics [4−7] and rigid flapping wing structure [8]. Ansari *et al* carried out an advanced study on the rigid flapping wing geometry using a nonlinear aerodynamic model [9]. The result indicates that a wing with more area outboard will enhance the wing performance. An experimental study on the effect of Aspect Ratio (AR) on the wing performance suggests that the wing with AR of 12 produces a higher value of lift force [10].

The effect of wing deformation on the performance of the flapping wing has been investigated using computational and numerical approaches. Du and San [11] pointed out the importance of wing deformation by using the wing kinematics measurement of Walker *et al* [12]. Their result shows that chord wise camber increases the lift, while the span wise twist reduces the power consumption. The three−dimensional numerical analysis on the effect of wing deformation reveals that the highly flexible wing augments the overall aerodynamic performance of the flapping wing [13]. Truong *et al* incorporated the unsteady blade element theory (UBET), and achieved a significant rise in the vertical force and reduction in the power consumption using a wing with a passive twist [14]. In addition, the experimental and numerical study of Tommy *et*

al on the flapping wing flight also demonstrates that the flexible wing improves the wing efficiency [15].

Although numerous studies have been conducted on the FWMAV, little work has been carried out on the experimental optimization of the flapping wing. Using the surrogate-based approximation of the unsteady aerodynamic loads, Gogulapati *et al* achieved the peak performance of the flexible wing by reducing the amount of the pitch actuator [16]. Nan *et al* conducted an experimental study to analyze the effect of wing shape on the wing performance [17]. The best wing performance is achieved with a trapezoidal wing shape and an AR of 9.3. Chaudhuri *et al* applied a multi-objective experimental optimization for the flexible flapping wing and improved the wing performed by maximizing the AR [18]. Most of the above-mentioned optimizations are conducted based on the kinematic parameters or wing components rather than considering just the wing geometric parameters. In nature, insect's wing with different combination of wing geometric parameters produces variable degree of aerodynamic performance. Therefore, there is still a need for further work on the optimization of the flapping wing based on wing geometric parameters.

1.2 Outline of thesis

The objective of this study is to optimize the flapping wing design for an efficient flight of the FWMAV. The main goal of this research is to maximize the power efficiency (thrust/power) of the flapping wing while still producing the sufficient amount of thrust force for the hover flight.

In this study, first, the effect of wing geometric parameters on the mean thrust generation, power consumption and power efficiency (thrust/power) is investigated by varying one geometric parameter at a time. The wing geometric parameters considered in this study are wing area, camber angle, non-dimensional radius of second moment of area and aspect ratio. Then, a surrogate based experimental design optimization is employed to optimize the flapping wing. A noisy Kriging model is constructed as the surrogate to consider the noise in the experimental data. We use EFI as an infill criterion, as it suggests a new point within the feasible region of the design space. The testing and manufacturing error in the experimental data is quantified as suggested by Viana *et al* [19]. The power efficiency of the optimized wing is calculated and compared with the other wings. At the end, the flight capability of the optimized wing is validated by carrying out a wired flight with stabilizer.

Chapter 2

Flapping mechanism, wing geometric parameters and experimental setup

2.1 Flapping mechanism

The flapping mechanism used in this experimental study has a simple design. This mechanism, which is driven by the blushed motor (BLH2402, Blade Co., USA), converts the rotational motion of the motor shaft into the flapping motion. It has three inner gears, colored red and blue, and two outer gears, colored brown (see figure 2.1). Inner blue gears are attached to the outer brown gears using a glue. Leading edge bar, made of 1 mm diameter carbon fiber reinforced polymer (CFRP), is mounted on the pocket hole of the inner and outer gear combined structure. Here, the red gear, which is driven by the blushed motor, drives the combined structure of inner blue and outer brown gear in an alternate fashion, which mimics the flapping motion of the flying insects.

By using this flapping mechanism, we can generate a large flapping angle within a limited space. When the flapper is flapping at 17.65 Hz of flapping frequency, flapping angle is around 165^0. The

maximum flapping angle recorded is around 178^0 when the flapper was flapping around 30.77 Hz. As mean thrust generation in the hover flight is directly proportional to the flapping amplitude, a higher value of flapping angle is beneficial for the FWMAVs.

The flapping mechanism consists of several parts. First, the 3D design of each parts is modeled in CAD. Then, CNC is used to mill these designs in a carbon plate (Carbon make Co., Korea). Finally, each part is attached one above the other using 0.8 mm steel rod and glue. The flapper is 25.6 mm in length and 28 mm in width. It weighs 8.3 g with wings and other structures.

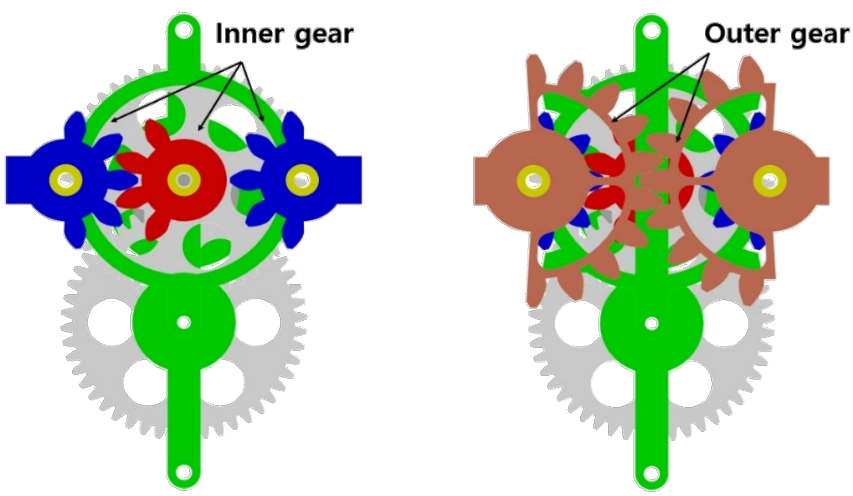

Figure 2. 1 Schematic of the flapping mechanism

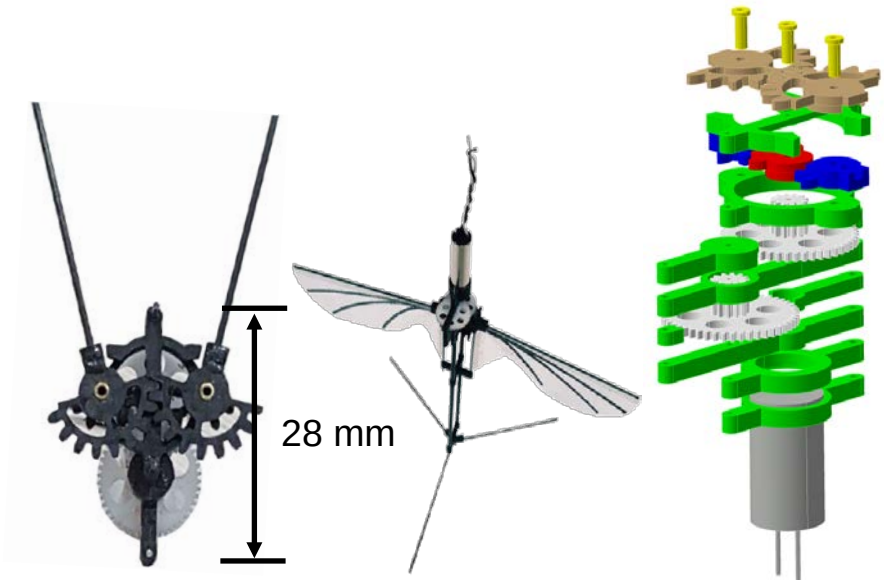

Figure 2. 2 Fabricated flapping mechanism

2.2 Wing Geometric Parameters

In nature, different insects have a distinct combination of wing geometric parameters. Insects flapping wing with different wing geometric parameters produces different degree of aerodynamic performance. Therefore, to find the best blend of the wing geometric parameters for our Flapping Wing Micro Air Vehicle (FWMAV), we first studied the effect of these wing geometric parameters on the aerodynamic performance by varying one geometric parameter at a time. The wing geometric parameters investigated in our experiment are wing area (S), camber angle (θ), non-dimensional second moment of area ($\hat{r}_2$) and Aspect Ratio (AR).

2.2.1 Wing area (S)

In our experiment, wing area S is defined as the planform area of the single wing.

2.2.2 Camber angle (θ)

Camber angle is simply defined as an angle between a line normal to the leading edge of the wing and the edge of wing root. Variation of camber angle alters the chord wise orientation of the wing along the wingspan, which affects the local angle of attack and the twist angle of the flapping wing.

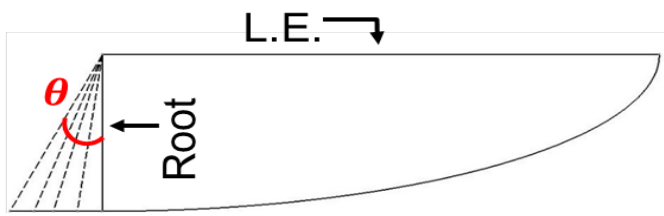

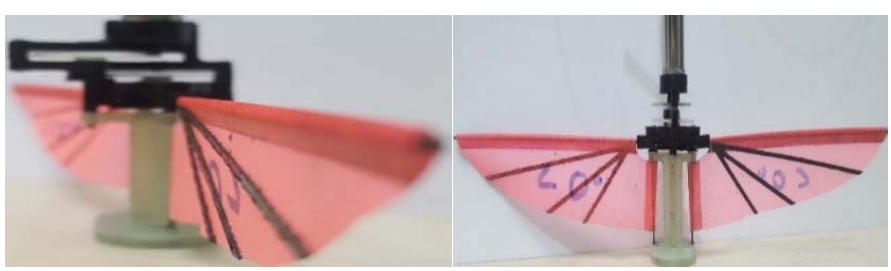

(a) 0^0 Camber angle

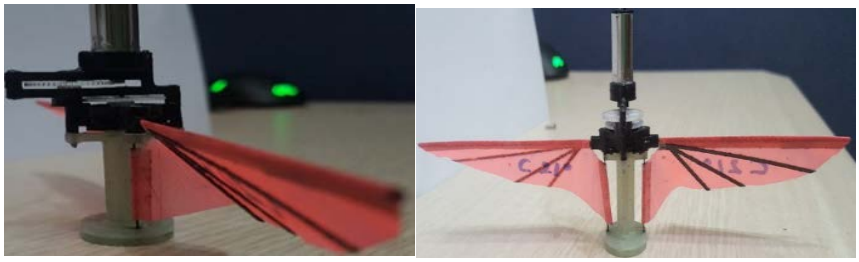

(b) 21^0 Camber angle

Figure 2. 3 Wing shape at different camber angle

2.2.3 Non-dimensional radius of second moment of wing area ($\hat{r}_2$)

Second moment of wing area reflects how the wing area is distributed along the wing axis. The second moment of wing area S_k is defined as

$$S_2 = 2\int_0^R cr^2 dr \ = SR^2 \int_0^1 \hat{c}\hat{r}^2 \, d\hat{r} \qquad (2.1)$$

where $\hat{c} = \frac{c}{\bar{c}}$ is the normalized chord length and $\hat{r} = \frac{r}{R}$ is a non−dimensional radius.

Finally, the non−dimensional radius of second moment of wing area [20]can be obtained by

$$\hat{r}_2^2 = \frac{S_2}{SR^2} = \int_0^1 \hat{c}\hat{r}^2 d\hat{r} \quad (2.2)$$

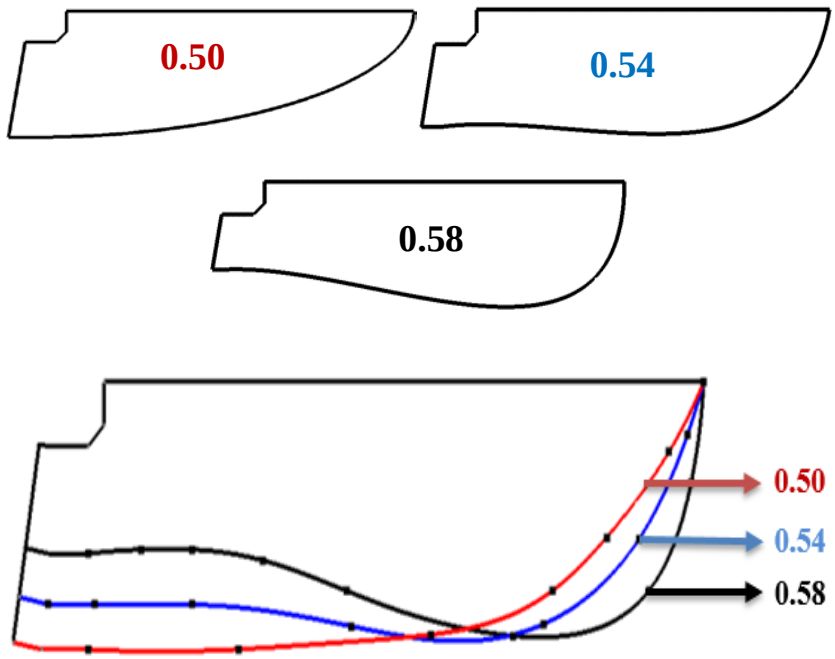

Figure 2. 4 Wing shape with different non-dimensional radius of second moment of area ($\hat{r}_2$).

2.2.3.1 Cubic Bezier Curve

In this study, a cubic Bezier curve is used to design the wing planform shape. Four control points (P_0, P_1, P_2, P_3) and Bernstein basis polynomial, which is given by Equation (2.3), are used to construct a cubic Bezier curve. Here, P_0 and P_3 are the known parameters. The value of y_0 of $P_0(0,y_0)$ is equal to the root chord length while the value of x_3 of $P_3(x_3,0)$ is equal to the span length.

$$B(t) = (1-t)^3 P_0 + 3(1-t)^2 t P_1 + 3(1-t)t^2 P_2 + t^3 P_3, t \in [0,1] \quad (2.3)$$

where, $P_0(0, y_0), P_1(x_1, y_1), P_2(x_2, y_2), P_3(x_3, 0)$ are the four control points of the Bezier curve. The coordinates of points $P_1(x_1, y_1)$ and $P_2(x_2, y_2)$ are found using a mathematical algorithm. And with these points, we can design the wing that will have the wing area of 1400 $mm^2$and the required value of $\hat{r}_2$.

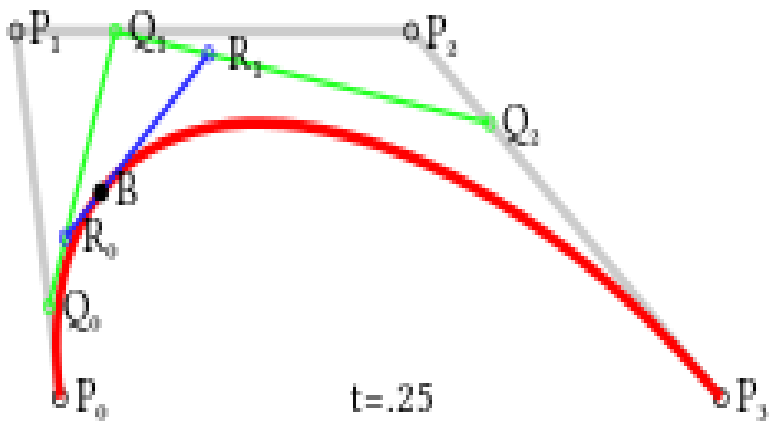

Figure 2. 5 Construction of cubic Bezier curve

2.2.4 Aspect Ratio (AR)

Aspect Ratio (AR) of the flapping wing is defined by

$$AR = \frac{(2R)^2}{2S}, \text{ where R = span length} \qquad (2.4)$$

It has been claimed that changing the value of Aspect Ratio will vary the size and strength of leading edge vortex (LEV), which is the main source of higher value of thrust production in the hover flight.

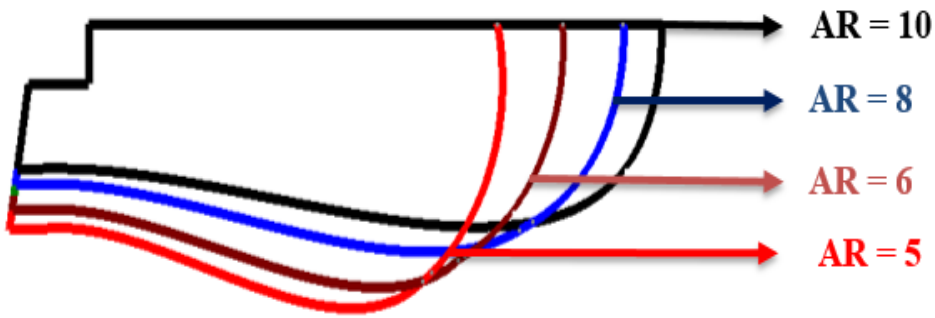

Figure 2. 6 Wing shape with different Aspect Ratio

2.3 Manufacturing of wing

The wing is made up of 15−micron thick high−tech polyester membrane (Oracover, LANITZ Co., Germany) and 0.10 mm thick Carbon Fiber Reinforced Polymer (Carbon make Co., Korea). Here, the wings are handmade. After fabricating the wing shape frame in a Delrin using a CNC, this frame is used as a guide to prepare a wing from a polyester membrane. The wing is cut using a sharp razor blade. Finally, the wing vein is attached to the wing membrane using a glue. In our experimental study, all the wings have the same vein orientation as shown in figure 2.7. In our initial vein test, this kind of vein shape produced the better aerodynamic performance.

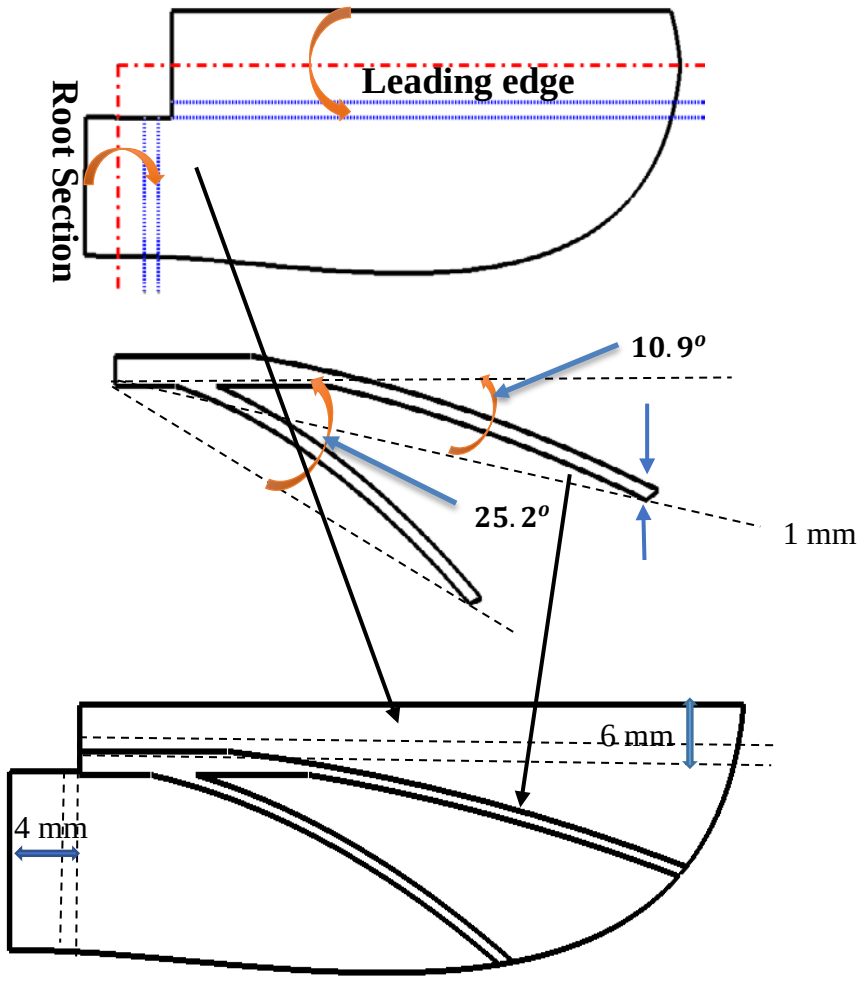

Figure 2. 7 Steps for wing production

2.4 Experimental Setup

To analyze the force and power experienced by the Flapping Wing Micro Air Vehicle (FWMAV), an experimental setup as shown in figure 2.8 is constructed. Here, the flapper with wing is mounted on a six-axis force and torque sensor (Nano 17, ATI Inc., USA). A

16-bit DAQ device (NI-USB-6251) is used to read the raw data of the sensor. At each flapping frequency, the data is collected at a sampling rate of 1 KHZ for 2.5 second and the thrust force at that flapping frequency is obtained as the average force over the 2.5-second time interval. Our experimental data is corrupted by the high frequency noise. To attenuate this high frequency noise, a second order Butterworth low pass filter is employed. At each sample points, the wing is tested ten times and the thrust produced by the wing is calculated as the mean of 10 measurements.

The input power is the power, product of input voltage and current, consumed by the motor to produce the required amount of flapping frequency. A Certain amount of input voltage is supplied from the DC power supply and the ammeter (8846a, FLUKE, USA) is used to measure the current flow. Power is also calculated as the mean of ten measurements. The power efficiency indicator is obtained as the ratio of average thrust force to the average power.

$$Power\ Efficiency = \frac{Average\ thrust\ force\ (gf)}{Average\ power\ (Watt)} \qquad (2.5)$$

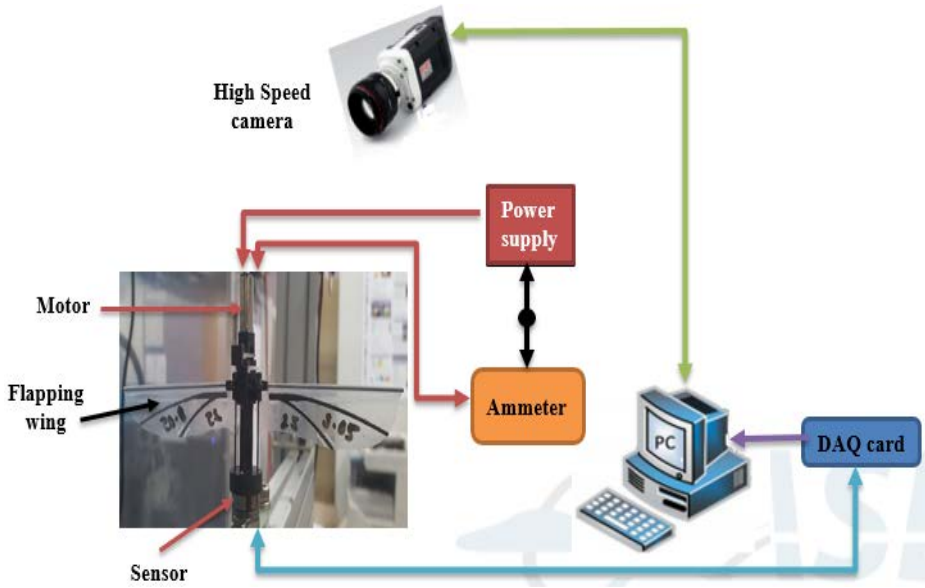

Figure 2. 8 Experimental setup for force and power measurement

Chapter 3

Methodology

3.1 Design of Experiment (DOE)

3.1.1 Central-Composite Design

The central composite design (CCD) is one of the most popular second order designs. In CCD, we have $2^{n_{dv}}$ factorial points, $2n_{dv}$ axial points, and n_c center run. In our DOE, we have three−design variable. Therefore, using CCD, we can reduce the number of design points to 15. Figure 3.1 shows the CCD with three design variables.

In CCD, the axial distance, α, varies from 1.0 to$\sqrt{n_{dv}}$. In our design space, we fixed it to 1.682. Center runs, n_c, more than 3 is a desirable case. Here, we use n_c = 6.

3.1.2 Design Space

To carry out this experimental optimization, we took three design variables that can have significant influence on the performance of the flapping wing. In this optimization process, we fixed the wing area to the constant value of 1400 mm^2. Based on the

results of the parametric study, we fixed the lower and upper bound of these design variables.

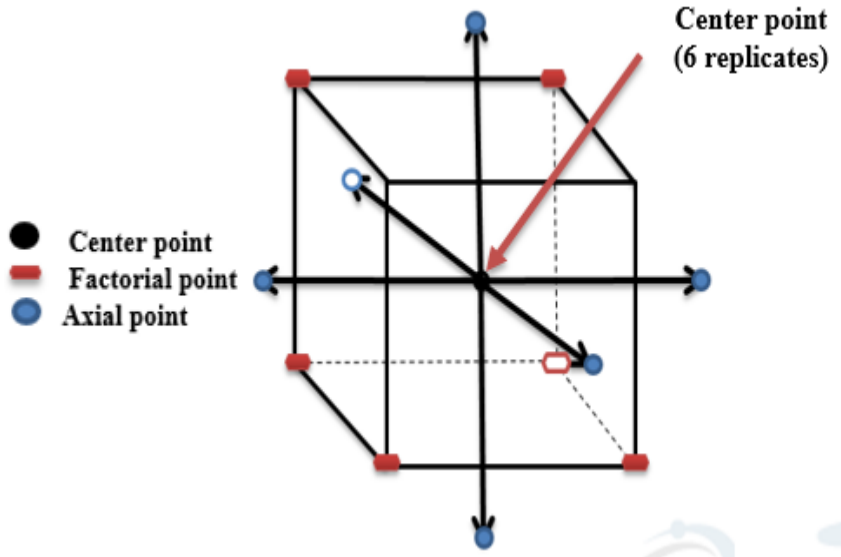

Figure 3. 1 Central Composite Design for three design variables

Table 3. 1 Design variable

Design Variable	Lower bound	Upper bound
Camber angle (θ)	**0.61^0**	**12.38^0**
Non-dimensional radius of second moment of wing area ($\hat{r}_2$)	**0.4727**	**0.6072**
Aspect Ratio (AR)	**5.14**	**9.35**

3.2 The Kriging model

In the aerodynamic shape design optimization, Kriging model is one of the popular meta-modeling technique. The kriging model can interpolate the sample data with high accuracy even in the noisy and non-linear case.

3.2.1 Ordinary Kriging

In the case of Ordinary Kriging, the response of interest y is given as

$$y(X) = \mu + Z(X) \tag{3.1}$$

where μ is an unknown constant value, and $Z(X)$ is a stationary Gaussian process. The covariance matrix and the Gaussian correlation function (R) between two design points are given by

$$Cov\left[Z(X^i), Z(X^j)\right] = \sigma^2 \mathbf{R}[R(X^i, X^j)], \tag{3.2}$$

$$R(X^i, X^j) = \exp[-\textstyle\sum_{k=1}^{n_{Dv}} \theta_k \left|X_k^i - X_k^j\right|^2] \tag{3.3}$$

where $\mathbf{R}$ is the correlation matrix and θ_k is an unknown correlation parameter. $\left|X_k^i - X_k^j\right|^2$ represents the distance between the k^{th} components of the sample points. After calculating the correlation

function at all the design points, the predicted value, $\hat{y}(x)$, and the variance, s^2, are given by

$$\hat{y}(X) = \hat{\beta} + r^T(X)\mathrm{R}^{-1}(y - \hat{\beta}f) \tag{3.4}$$

$$s^2(X) = \sigma^2 - r^T\mathbf{R}^{-1}r + \frac{(1-f^T\mathbf{R}^{-1}r)^2}{f^T\mathbf{R}^{-1}f} \tag{3.5}$$

with

$$\hat{\beta} = (f^T R^{-1} f)^{-1} f^T \mathbf{R}^{-1} y \tag{3.6}$$

$$r^T(X) = [R(X, X^1), R(X, X^2), \ldots, R(X, X^{n_s})]^T \tag{3.7}$$

$$\hat{\sigma}^2 = \frac{(y-\hat{\beta}f)^T\mathbf{R}^{-1}(y-\hat{\beta}f)}{n_s} \tag{3.8}$$

where y is a column vector with length equal to the number of sample points, f is a unit vector with dimension equal to the number of sample points. $r^T(X)$ is the correlation vector between the added point and the sample points.

3.2.2 Kriging with noisy observation

While measuring the experimental data, the user will not get the true value of the observation but will have only access to the noisy observation, which is of the form

$$\breve{y}_i = y(X)^i + \varepsilon_i \tag{3.9}$$

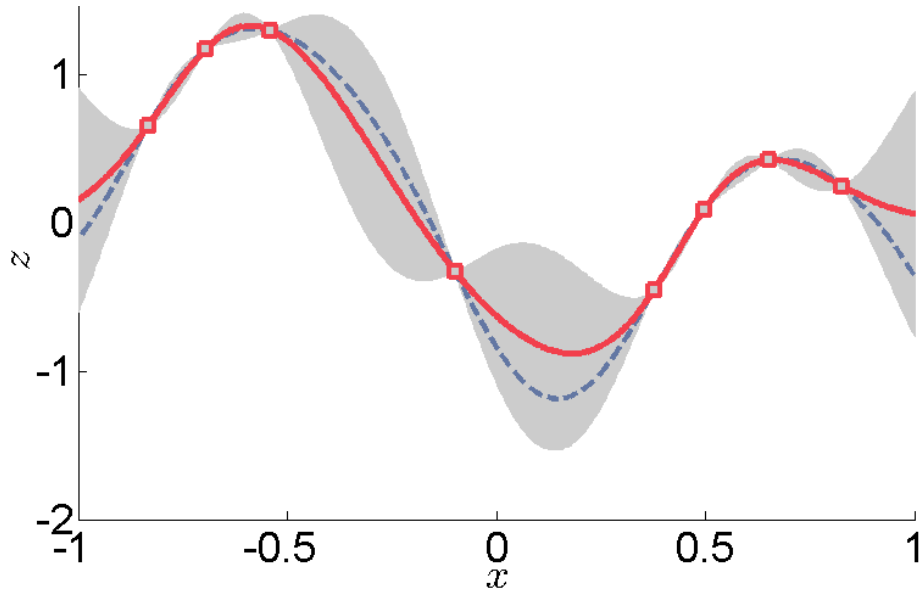

Figure 3. 2 Ordinary Kriging model

where ε_i is a random noise variable. Here, the predicted value, y(X), and the variance, s^2, are similar to that of the ordinary Kriging but the only difference is in the kernel function R, which is replaced by $\mathrm{R} + \tau^2 \boldsymbol{I}$. τ^2 is the variance of the noise. Figure 3.2 shows the noisy Kriging model. Unlike ordinary Kriging, where the predicted value is an interpolated value from each observation, noisy Kriging model does not interpolate the noisy measurements. In the noisy case, the variance is non−zero at each design point.

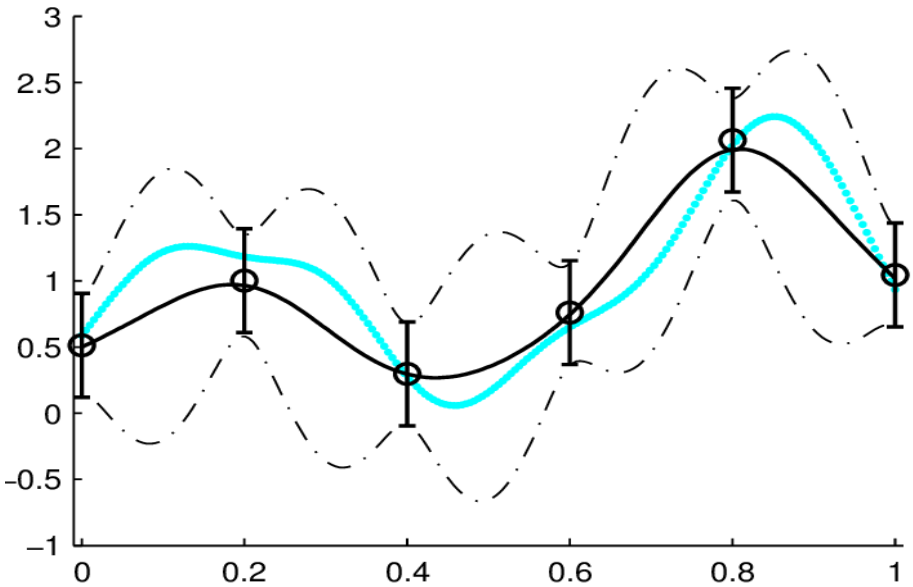

Figure 3. 3 Kriging with noisy observation

3.3 Infill Criteria

A so-called infill criteria is used to find the global optimum point within the given design space. After constructing the kriging model, the infill criterion extracts the information from the model and predicts the new design point for the further evaluation.

3.3.1 Expected Improvement

For the kriging based optimization problem, Expected Improvement (EI) is one of the popular infill criterion. EI predicts the

new point by considering both the predicted value and the uncertainty of the predicted value from the kriging model. The basic idea of EI is

$$I(X) = \begin{cases} y_{min} - \hat{y}(x), & if\ \hat{y} < y_{\min} = \max[y_{min} - \hat{y}(x), 0] \\ 0 & , otherwise \end{cases} \quad (3.10)$$

$$E[I(X) = (y_{min} - \hat{y})\Phi\left(\frac{y_{min} - \hat{y}}{s}\right) + s\phi\left(\frac{y_{min} - \hat{y}}{s}\right) \quad (3.11)$$

where y_{min} is the current minimum and $\hat{y}$ is the predicted value at each design point. Φ is the Gaussian cumulative distribution function and ϕ is the Gaussian cumulative density function. In our optimization process, we deal with constrained optimization. Programming language R offers an extension of the function max_EI for the constrained optimization as crit_EFI. By using this function, we can compute the Expected Feasible Improvement at the current feasible location.

3.4 Estimating testing and manufacturing uncertainties

In the experimental process, several sources vary the experimental data. In this experimental investigation, we consider testing and manufacturing uncertainty as the major sources of variability. The presence of noise in the sensor varies the measurement. The difference in the testing condition also increases

the testing uncertainty. Manufacturing uncertainty is mainly due to the human error while manufacturing the wings.

In this experimental analysis, each wing is tested ten times. To quantify the testing uncertainty, the mean of ten measurements is calculated as shown in Equation (3.12) and then, for the same wing, the standard error of the sample mean is used, which is given by Equation (3.13).

$$Mean^{(i)} = \frac{1}{n}\sum_{j=1}^{n} T_j \text{ , where n = 10} \qquad (3.12)$$

$$SE\left(Mean^{i}\right) = \sqrt{\frac{\sum_{j=1}^{n}(T_j - Mean^{(i)})^2}{n^2 - n}} \qquad (3.13)$$

Normally identical wings can generate different value of mean thrust force. To consider the manufacturing variability, six replicates of the center point of the central composite design (CCD) is constructed and each replicate is tested ten times. First, for each replicated wing the average value of the ten measurements is measured and then the mean of six replicated wings is calculated as

$$\overline{Mean}^{(cp)} = \frac{1}{d}\sum_{j=1}^{d} Mean_j^{(cp)}, \text{ where d = 6} \qquad (3.14)$$

and the standard error of the mean of center point replicates $\overline{Mean}^{(cp)}$ is given as

$$\text{SE } (\overline{Mean}^{(cp)}) = \sqrt{\frac{\sum_{j=1}^{d}(Mean_j^{(cp)} - \overline{Mean}_j^{(cp)})^2}{d^2 - d}} \qquad (3.15)$$

At the center point in our design space, we calculated the manufacturing error by making its six replicates. However, we have large number of design points in the design space, so calculating the manufacturing error at each design points by making their six replicates is not feasible. Therefore, to limit the number of experiments, we assumed that the manufacturing error measured at the center point is same at all the design points.

Now, the total uncertainty in the design space is calculated as the sum of testing uncertainty, which is the average value of the standard error over all the design points, and manufacturing uncertainty.

$$\hat{\sigma}_n^2 = \hat{\sigma}_n^2|_{testing} + \hat{\sigma}_n^2|_{manufacturing,} \qquad (3.16)$$

$$\hat{\sigma}_n^2|_{testing} = \frac{\sum_{i=1}^{d_n}(SE(Mean^i))^2}{d_n}, \text{ and} \qquad (3.17)$$

$$\hat{\sigma}_n^2|_{manufacturing} = \frac{\sum_{i=1}^{r_n}(SE(\overline{Mean}^i))^2}{r_n} \qquad (3.18)$$

where d_n is the number of design points and r_n is the number of design points for which identical wings are available. When we

analyze the standard deviation of the power efficiency, we found out that this value is random at all the design points. Therefore, we assumed that the total uncertainty is same at all the points in our design space.

Chapter 4

Results for parametric study

In this section, we analyze the experimental results obtained by varying wing geometric parameters. We compare the performance of various wing designs based on the mean thrust, power consumption, and power efficiency. For each wing design, the thrust force generation and the power consumption are measured at 13 Hz, 17 Hz, 21 Hz and 24 Hz. In the case of camber angle, we also analyzed the wing performance at 26 Hz. In our experimental study, we need to collect a large number of experimental data. However, when operating at high flapping frequencies like 26 Hz and 28 Hz, some of the wings suffered structural failure and the motor showed a reduction in its performance because of the rise in temperature. Interestingly, the mean thrust generation and power consumption showed the similar trend at 24 Hz and 26 Hz of flapping frequency. Therefore, to make the data collection more effective, the data are measured only at 13 Hz, 17 Hz, 21 Hz and 24 Hz for other families of the wing.

4.1 Wing area

The aim of this study is to analyze the effect of changing the wing area on the wing performance. The wing planform shape is semi−ellipse. Here, the wing area is changed from 800 mm^2 to 1740 mm^2 while the Aspect Ratio is kept constant. Figure 4.1 (a) shows that mean thrust force increases with the increase of wing area. The thrust vs frequency plot also indicates that the mean thrust force generation is proportional to the flapping frequency. At 21 Hz of flapping frequency, wing with a wing area of 800 mm^2 produces 2 gf of thrust, while wing with an area of 1700 mm^2generates 16 gf of thrust force. This result indicates that increasing the wing area is better for thrust generation in hover flight.

In Flapping Wing Micro Air Vehicle (FWMAV), the power supply is very limited. Therefore, in addition to generating enough amount of thrust force for the hover flight, the perfect FWMAV should also be power efficient. When we compare the power efficiency plot (see figure 4.1 (b)) at a low flapping frequency, wing with large wing area produces a higher value of power efficiency. However, with the increase of flapping frequency, wing with a wing area of 1480 mm^2 and 1700 mm^2 shows a rapid decline in the power efficiency. Although wing with area of 1400 mm^2 produces a lower value of mean

thrust force than the wing with an area 1480 mm^2 and 1700 mm^2, it.

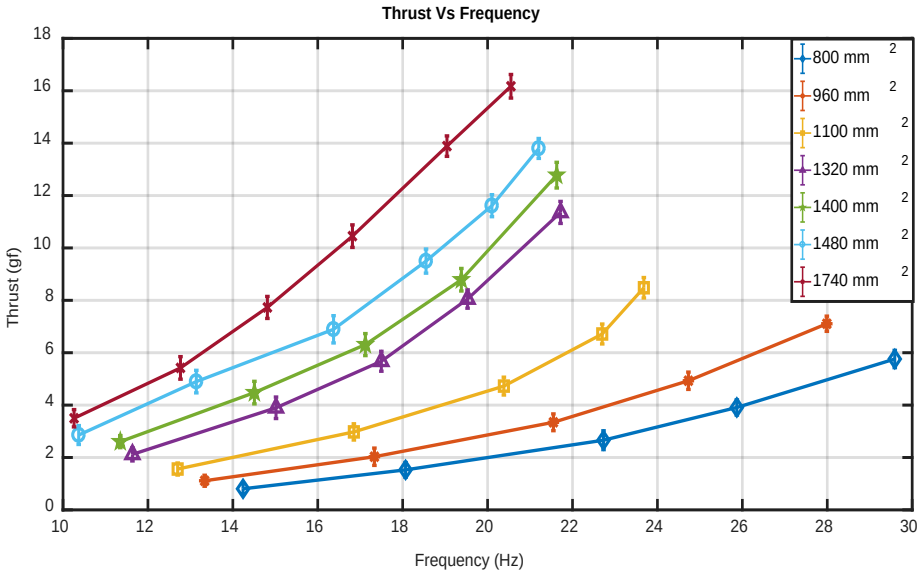

(a) Thrust vs Frequency

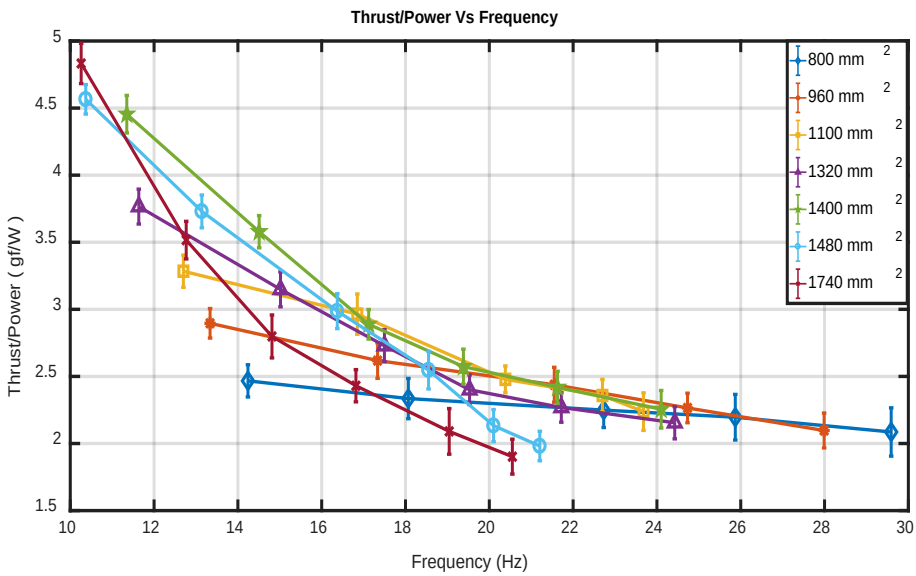

(b) Thrust/Power vs Frequency

Figure 4. 1 Effect of wing area on mean thrust generation and power consumption

shows better power efficiency than any other wing at all flapping frequency. The aim of this experimental investigation is to maximize the power efficiency while still generating the sufficient amount of thrust force for hover flight. As wing with area 1400 mm^2 fulfils both the requirements, this wing will be used for further investigation.

4.2 Camber angle

To investigate the effect of camber angle on the performance of the flapping wing, the camber angle is varied between 0^0 to 24^0 while the wing area is kept to a constant value of 1400 mm^2. Figure 4.2 shows the effect of changing the camber angle on the mean thrust production. When we compare the wing performance at the low flapping frequency, we can see that the mean thrust generation increases with the rise of the camber angle and it reaches the maximum when the camber angle is around 10^0. However, at high flapping frequencies, like 21 Hz – 26 Hz, highly cambered wings show a significant drop in the thrust production. At these frequencies, the wing with camber angle of 6^0 produces a higher value of mean thrust force than any other wings.

From figure 4.3 (a), we can see that the wing with a lower value of camber angle consumes more power than a highly cambered wing.

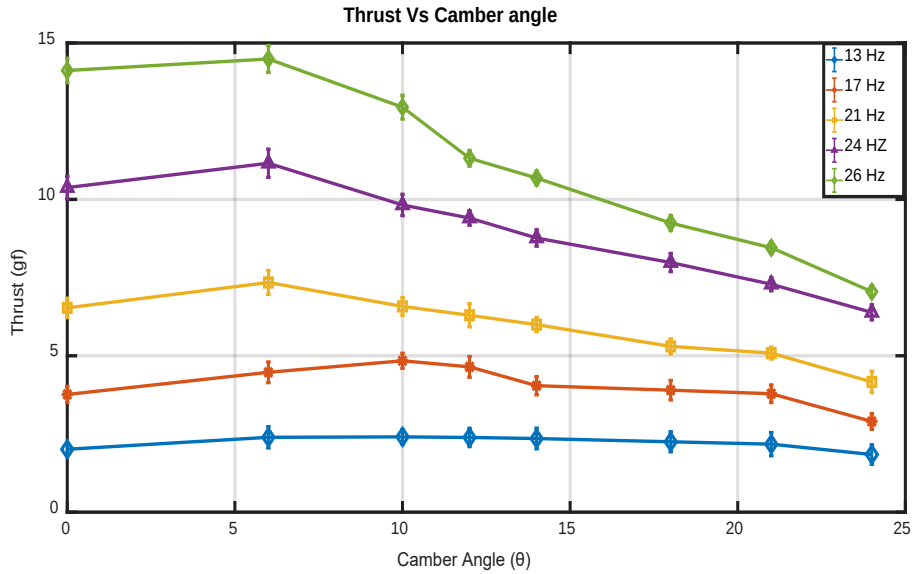

Figure 4. 2 Effect of camber angle on mean thrust generation

The plots for thrust to power ratio (see figure 4.3 (b)) shows that power efficiency increases with the increase of camber angle and this value reaches the peak when the camber angle is 10^0. Although, 6^0camber angle wing is an ideal wing in terms of thrust generation it lags behind 10^0 camber angle wing when power efficiency is taken into account. The highest power efficiency is achieved with 10^0 camber angle wing and as this wing also generates a reasonable amount of mean thrust force, this wing is selected as an ideal wing from this family.

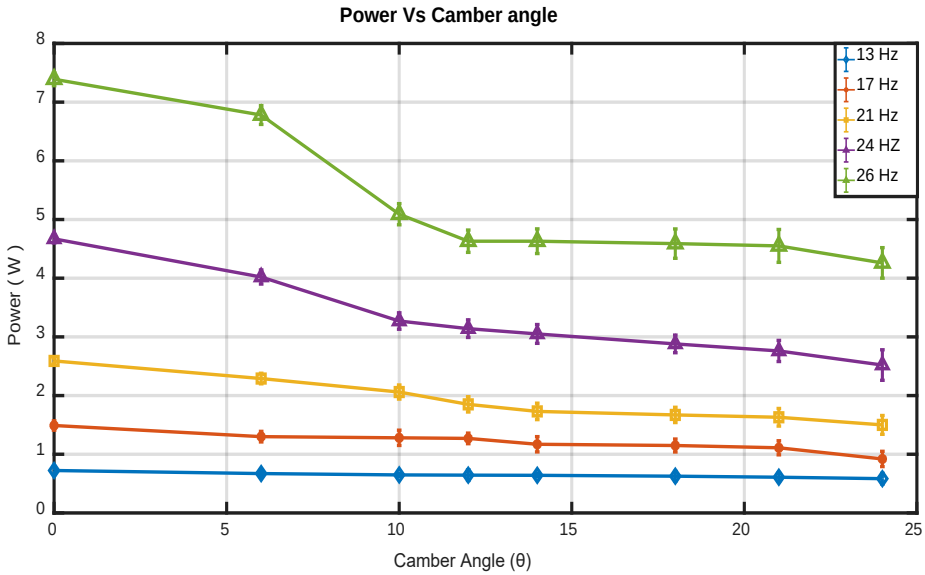

(a) Camber angle vs Power consumption

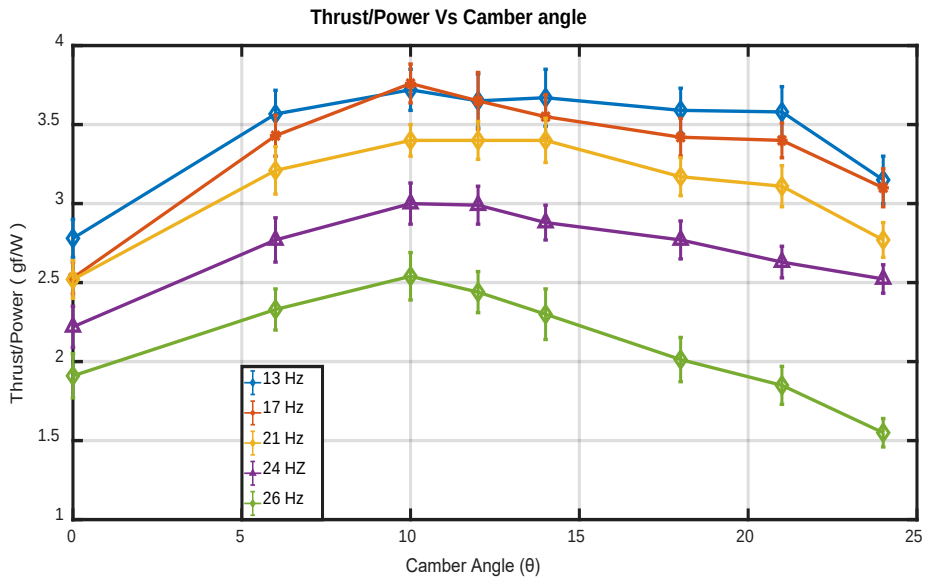

(b) Camber angle vs Power efficiency

Figure 4. 3 Effect of camber angle on mean thrust generation and power efficiency

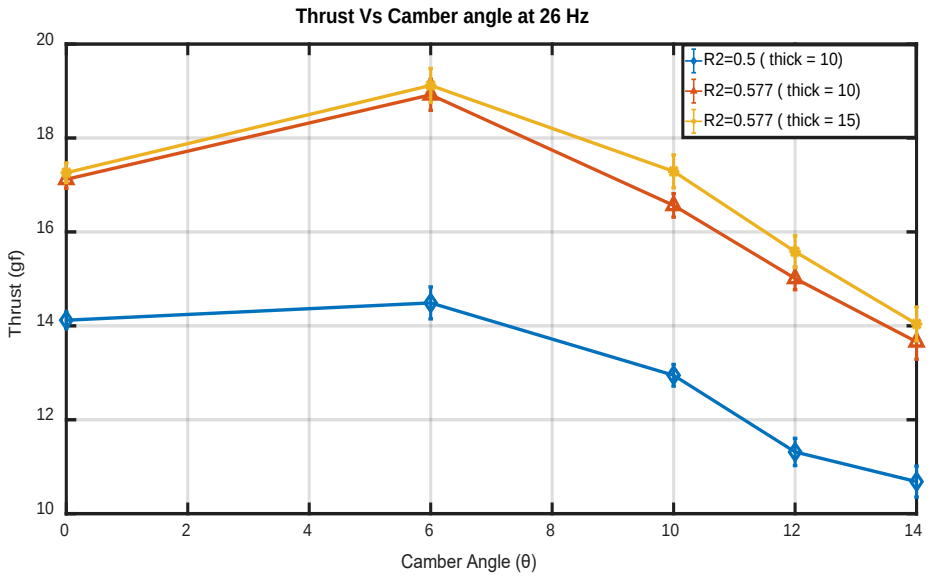

Figure 4. 4 Comparison of effect of camber angle on mean thrust generation for different wing shape

To see if the above results of the camber angle hold for different wing feature, we change the wing shape from semi−ellipse ($\hat{r}_2$ = 0.50) to paddle shaped ($\hat{r}_2$ = 0.577). Additionally, we also change the thickness of the wing membrane from 10 μm polyester fiber to 15 μm polyester fiber. As noted earlier, 6^0 camber angle wing produced a higher value of mean thrust force (see figure 4.4) and the maximum power efficiency is achieved when the camber angle is 10^0 (see figure 4.5 (b)). From this study, it proves that the effect of the camber angle on mean thrust generation and power efficiency is same for all the wing features. To generate a higher amount of thrust force, our flapping wing needs to operate at the high flapping frequency. At

high flapping frequency, the wing made from 15−μm polyester fiber

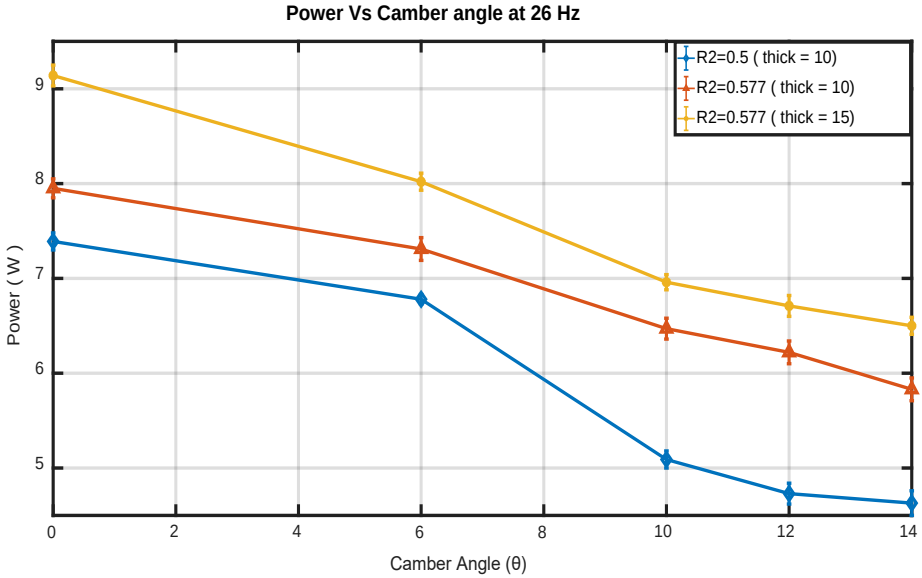

(a) Camber angle vs Power consumption

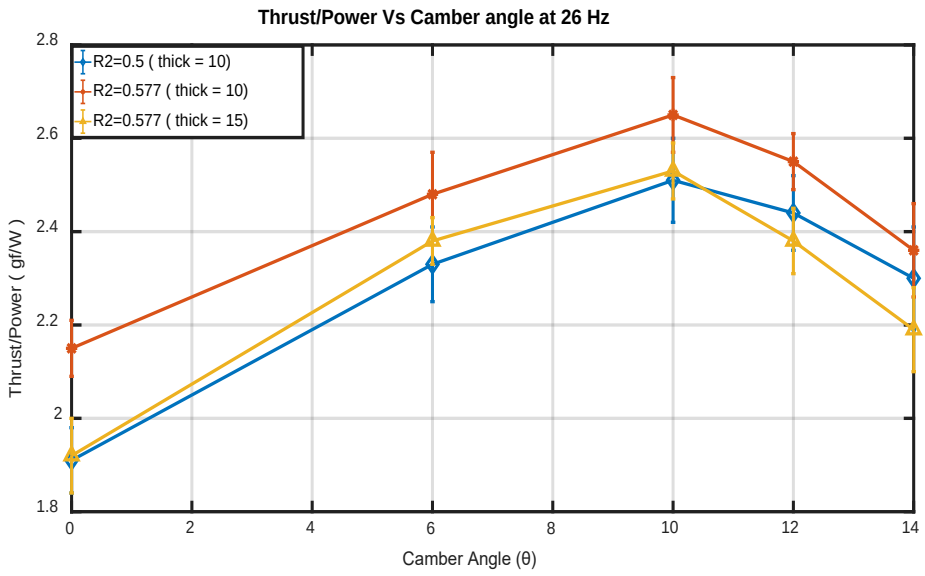

(b) Camber angle vs Power efficiency

Figure 4. 5 Comparison of effect of camber angle on power consumption and power efficiency for different wing shape

showed less structural failure than the wing with 10−μm thickness. Therefore, from here, we manufacture the wing using 15 μm thick polyester fibers.

4.3 Non-dimensional radius of second moment of wing area ($\hat{r}_2$)

The effect of non−dimensional radius of second moment of wing area ($\hat{r}_2$) is investigated by changing $\hat{r}_2$ from 0.50 to 0.58 while keeping the wing area and camber angle constant. Figure 4.6 shows the effect of $\hat{r}_2$ on mean thrust force generation. The result shows that mean thrust force generation increases with the increase of $\hat{r}_2$ and it reaches the peak value when $\hat{r}_2$ is 0.58. From a quasi−steady perspective, thrust force is proportional to the wing area and flow velocity. Increasing $\hat{r}_2$ pushes the wing area more towards the tip, where the flow velocity is high. Therefore, mean thrust generation increases with the increase of $\hat{r}_2$. Although increasing the value of $\hat{r}_2$ beyond 0.58 is possible, doing so will reduce the root chord length. From the structural point of view, a wing with shorter root section is not desirable as this wing can suffer from structural failure because of the high bending moment at the root section. Therefore, $\hat{r}_2$ = 0.58 is taken as the highest limit of $\hat{r}_2$ in our experimental study.

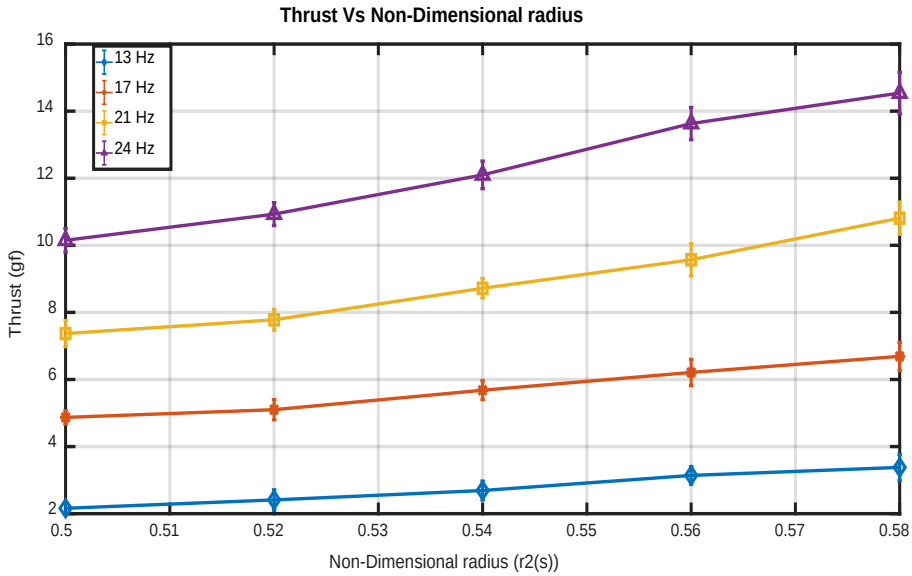

Figure 4. 6 Effect of non-dimensional radius on mean thrust generation

The effect of $\hat{r}_2$ on power consumption is quite similar to that of mean thrust generation (see figure 4.7 (a)). It shows that increasing $\hat{r}_2$ will increase the power consumption. Both the mean thrust and power rises with the increase of $\hat{r}_2$. However, the mean thrust generation is more rapid than the power consumption. Therefore, the power efficiency also rises with the increase of $\hat{r}_2$. As wing with $\hat{r}_2 = 0.58$ produces a higher value of thrust force and power efficiency than any other wings, this wing will be used for further investigation.

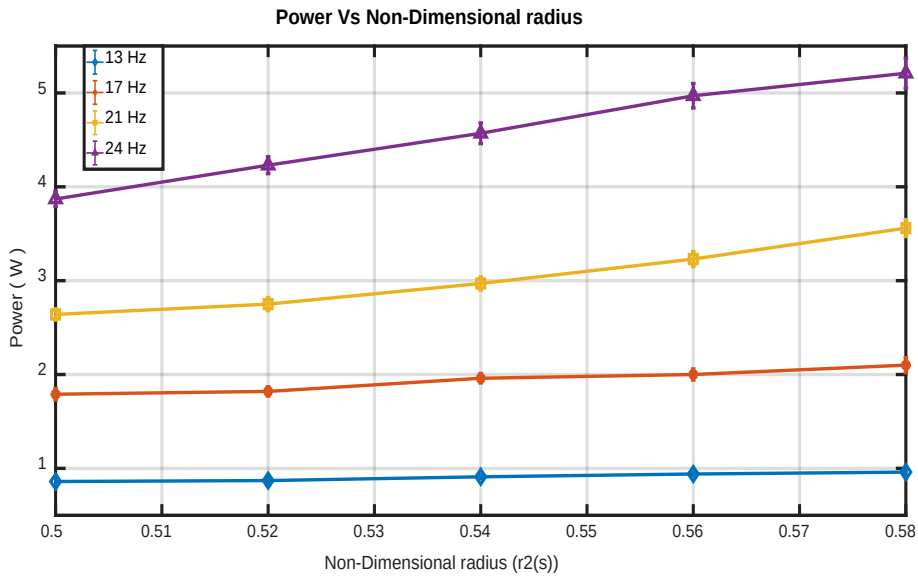

(a) Non-dimensional radius vs Power consumption

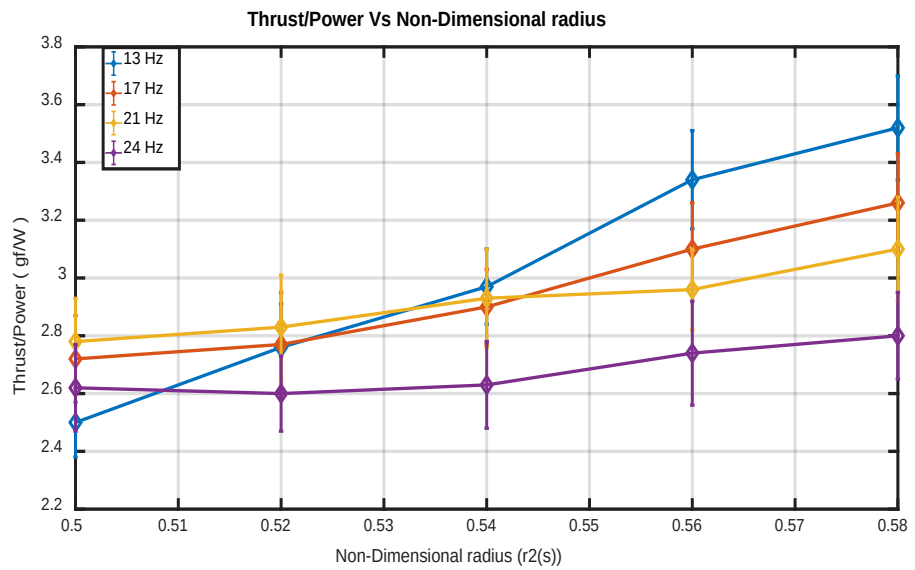

(b) Non-dimensional radius vs Power efficiency

Figure 4. 7 Effect of non-dimensional radius on power consumption and power efficiency

4.4 Aspect Ratio

The aim of this section is to analyze the effect of aspect ratio (AR) on the performance of the flapping wing. Here, we changed the AR from 5 to 10 while keeping the wing area, camber angle and $\hat{r}_2$ to their best value. At low flapping frequency, the mean thrust generation increases in a linear fashion with the increasing of AR (see figure 4.8). However, this trend is not common when the frequency is increased to a higher value. At 24 Hz, the mean thrust generation increases rapidly when the AR is increased from 5 to 8 but this rate slows down when the AR is increased beyond 8. It has been claimed that increasing the AR increases the size and strength of the LEV, which is the main source of thrust generation in hover flight, but when the AR is increased beyond the certain value, the LEV will break off and this will lower the thrust generation. In this study, a slower rate of mean thrust generation beyond the AR of 8 maybe because of the LEV breakdown.

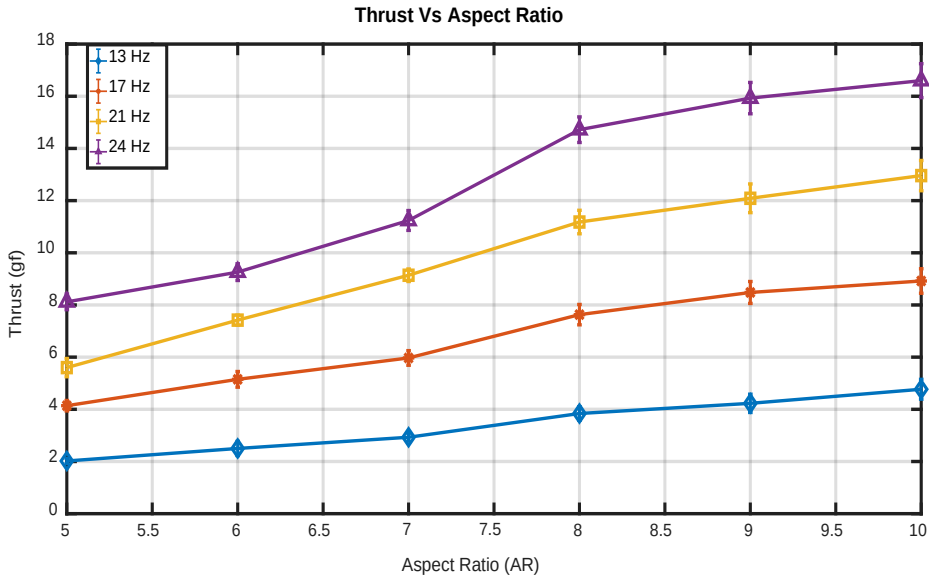

Figure 4. 8 Effect of aspect ratio on mean thrust generation

Figure 4.9 (a) shows that the effect of AR on power consumption is very similar to that of mean thrust generation. However, the plots for power efficiency versus AR present an interesting result. It shows that the power efficiency increases with the increase of AR and attains its peak when AR is 8. It also indicates that increasing AR beyond 8 has a detrimental effect on the power efficiency.

From this study, we can infer that if we want to design an efficient FWMAV, it is better to design the wing with an area of 1400 mm^2, camber angle of 10^0, $\hat{r}_2$ of 0.58 and AR of 8.

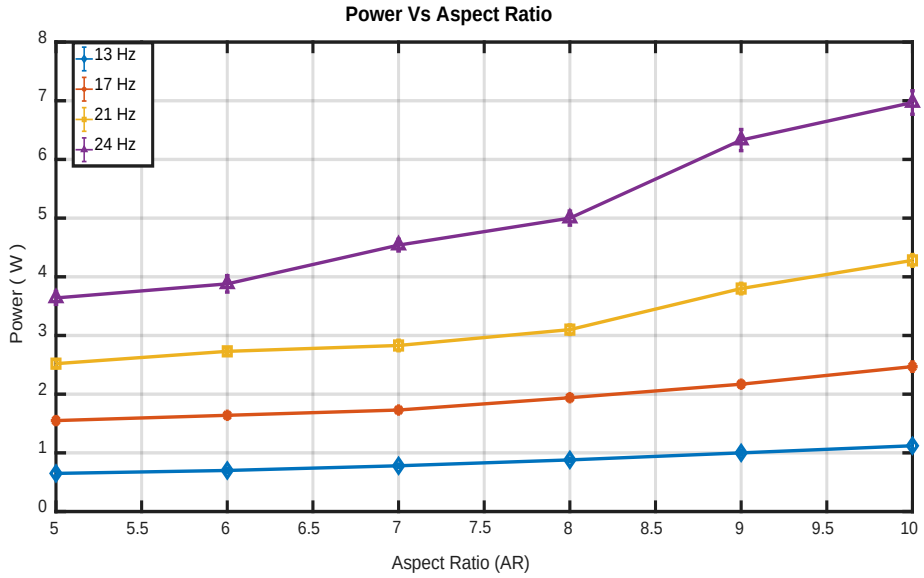

(a) Aspect Ratio vs Power consumption

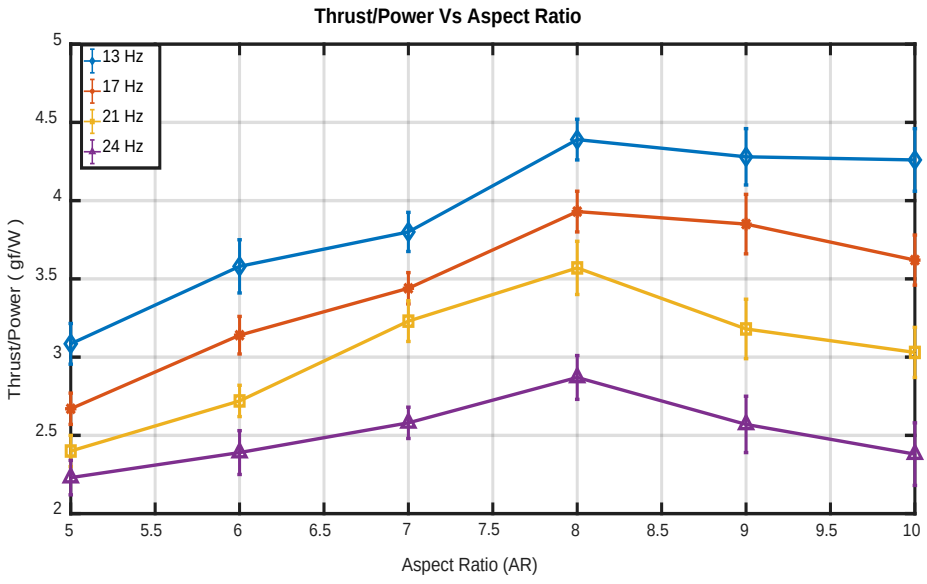

(b) Aspect ratio vs Power efficiency

Figure 4. 9 Effect of AR on power consumption and power efficiency

Chapter 5

Results for Experimental Design Optimization

In this experimental design optimization process, a genetic algorithm (GA) is used to find the global optimum point in our design space. First, a noisy Kriging model is constructed as the surrogate to consider the noise in the experimental data. Then, at each cycle, a new point is added using EFI – an extended version of EI. The objective function – Power efficiency –is calculated at the added new point and the surrogate is further updated using this new sample point. This process continues until a termination criterion is reached.

At each design point, ten measurements are taken at 24 Hz of flapping frequency. Then, the mean of these values is fitted for each design point. The total uncertainty for the power efficiency is 0.00024539. To carry out this optimization process, the programming language R is used. It provides DiceKriging function, to construct the Kriging model, and DiceOptim function, to find the optimum design points using several infill criteria.

5.1 Objective Function

The objective of this design optimization process (given by Equation 5.1) is to maximize the power efficiency (minimize the negative value of the power efficiency) of the flapping wing. The thrust force, greater than 13 gf, and root length, greater than 15 mm, are imposed as a constraint in this optimization process (see Equation 5.2 and 5.3). The thrust force of 13 gf is imposed to ensure that the optimized design will produce the sufficient amount of thrust force for the hover flight. The root length constraint would prevent the optimized wing from being too small at the root section. At high flapping frequency, wing with root length less than 15 mm usually suffers from structural failure at the root section.

$$Maximize: Power\ Efficiency = \frac{Thrust}{Power} \tag{5.1}$$

$$Constraints: Thrust > 13\ gf \tag{5.2}$$

$$Root\ Length > 15\ mm \tag{5.3}$$

5.2 Results and Discussion

15 design points are created using the central composite design (CCD). Table 5.1 shows the initial design points and their

mean experimental values. Figure 5.1 presents the power efficiency contour for the initial Kriging model with the CCD design points. The contour is constructed at AR of 8.25. It shows that a lower value of θ and $\hat{r}_2$ decreases the power efficiency, while a higher value of θ and $\hat{r}_2$ increases the power efficiency. Figure 5.2 and 5.3 shows the contour of the feasible and infeasible region for the root length and thrust constraints, respectively. In the first cycle, EFI suggests one new optimum design point. The thrust and power efficiency is measured at this new suggested point and the Kriging model is further updated using this new sample point. This process is continued for several cycles. Table 5.2 compares the predicted value with the mean experimental value at the five new added points. It shows that the mean experimental value is close to the surrogate prediction. It also indicates that our Kriging model is highly accurate. Among the five added point, the fifth point shows an improvement in the power efficiency. However, this improvement is not that significant. As there is no justifiable improvement in the power efficiency, we decided to terminate this expensive experimental optimization process after the fifth cycle.

Table 5. 1 Initial design points and their experimental results

Wing Design No.	θ	$\hat{r}_2$	AR	Experimental data (Mean value)		
				Thrust (gf)	Power (Watt)	Power Efficiency (gf/watt)
1.	3^0	0.50	6	6.0292	3.2788	1.8388
2.	10^0	0.50	6	7.1724	2.9106	2.4624
3.	3^0	0.58	6	7.1651	3.7880	1.8915
4.	10^0	0.58	6	9.0202	3.6114	2.4977
5.	3^0	0.5	8.5	7.9298	5.2730	1.5038
6.	10^0	0.5	8.5	10.9767	4.4935	2.4427
7.	3^0	0.58	8.5	13.7523	6.5061	2.1137
8.	10^0	0.58	8.5	15.9393	5.6684	2.8119
9.	0.61^0	0.54	7.25	7.5742	5.9124	1.2810
10.	12.38^0	0.54	7.25	10.2478	4.3784	2.3405
11.	6.5^0	0.4727	7.25	7.6192	3.7070	2.0553
12.	6.5^0	0.6072	7.25	11.1653	5.2669	2.1198
13.	6.5^0	0.54	5.14	7.3755	3.6687	2.0103
14.	6.5^0	0.54	9.35	13.8994	5.5168	2.5194
15.	6.5^0	0.54	7.25	10.5618	4.9317	2.1416

Table 5. 2 Comparison of the predicted value with the experimental value at the added new points

No. of new sample point	θ	$\hat{r}_2$	AR	Surrogate Prediction	Mean experimental value
				Power Efficiency	Power Efficiency
1.	9.472^0	0.567	9.1157	2.8226	2.7810
2.	8.9128^0	0.5836	8.7999	2.7983	2.8056
3.	7.92^0	0.5812	8.6113	2.8105	2.7709
4.	10.24^0	0.5851	8.6113	2.8094	2.8015
5.	9.5678^0	0.5876	8.2925	2.8056	2.8120

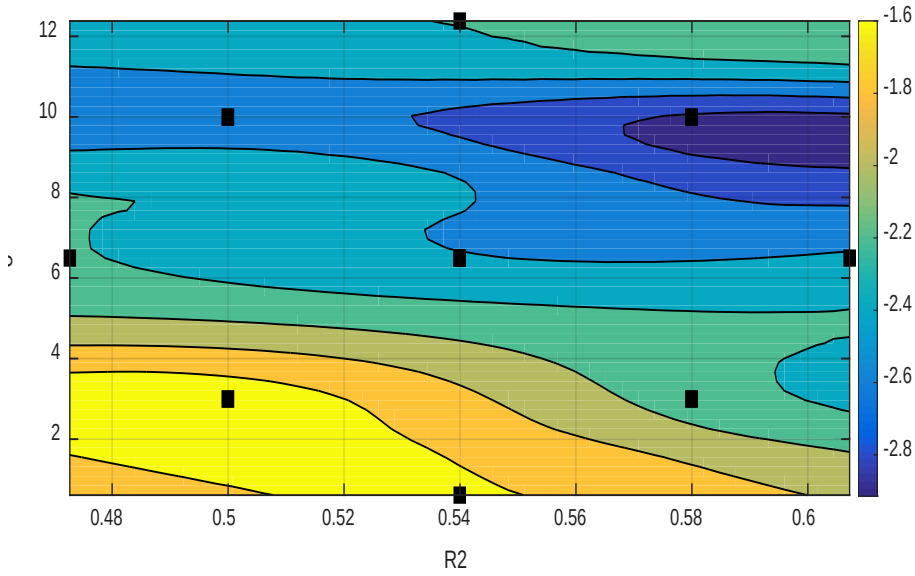

Figure 5. 1 Power efficiency contour by initial Kriging model

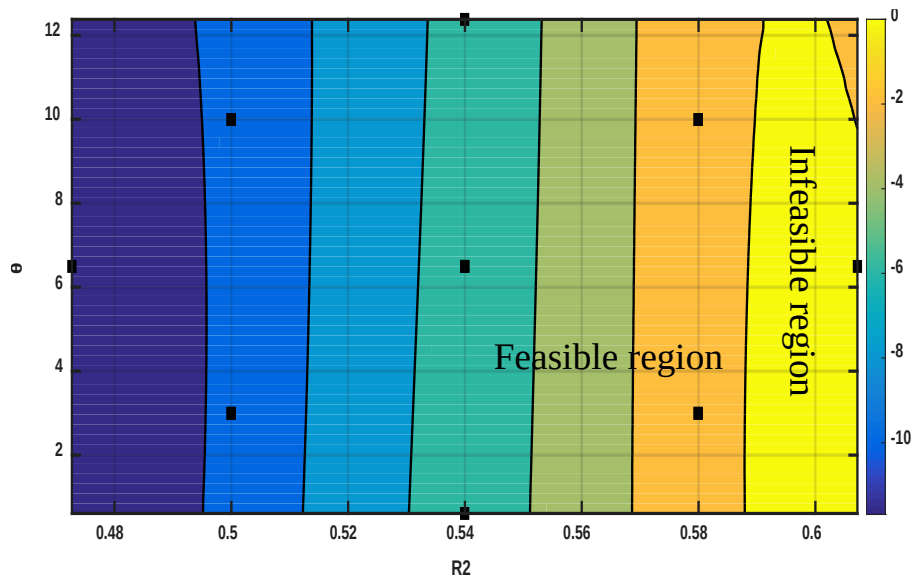

Figure 5. 2 Contour plot showing the feasible and infeasible region of the root length

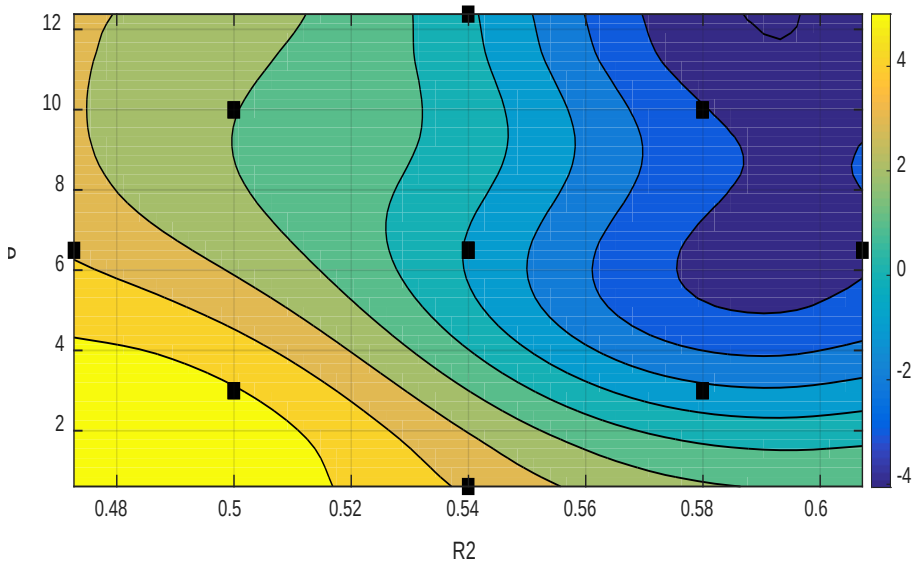

Figure 5. 3 Contour plot showing the feasible and infeasible region of the thrust

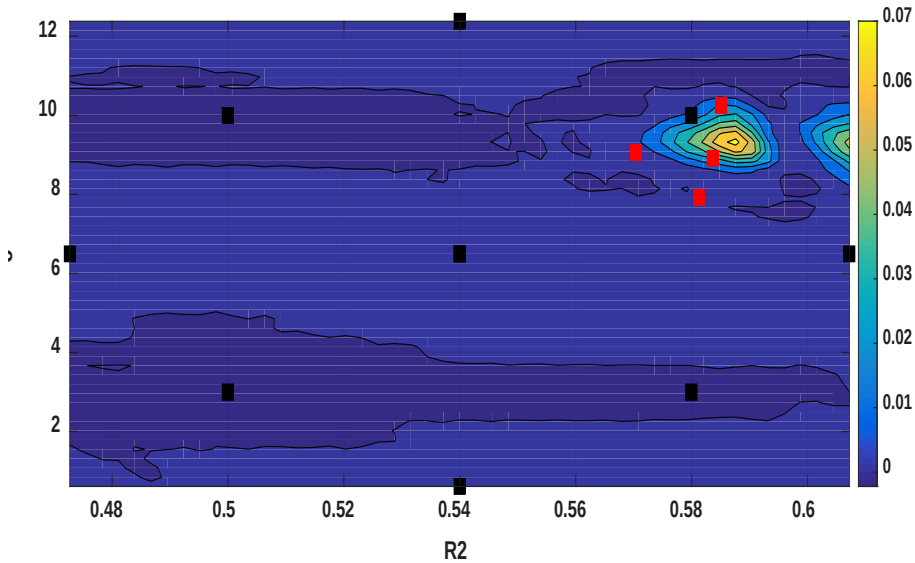

Figure 5. 4 Contour showing the added and suggested new points from EFI

5.3 Comparison of the power efficiency for the optimized wing with baseline design

The main aim of this section is to compare the power efficiency of the optimized wing with that of the baseline wing, which is a semi-elliptical wing with a camber angle of 0^0. Table 5.3 compares the power efficiency for the optimum wing geometry. The power efficiency of the baseline wing is 2.2552. From the parametric study, we are able to increase the power efficiency of the flapping wing to 2.7895, which is 23.69% greater than the baseline wing. Using the surrogate-based optimization process, the power efficiency of the flapping wing is increased to 2.8120 ± 0.0219. This power efficiency is 0.8 % higher than the wing from the parametric study. When we compare the power efficiency of the optimized wing, obtained from design optimization using kriging model, with the best wing from the parametric study, they show little difference in the objective function. It may suggest that the local minimum obtained from the parametric study is close to the global minimum in our design space.

Table 5. 3 Comparison of the power efficiency for the optimal wing geometry

	θ	$\hat{r}_2$	AR	Objective function (Power efficiency)
Baseline wing	0^0	0.50	6	2.2552
Best wing (Parametric study)	10^0	0.58	8	2.7895
Optimum Wing (Design Optimization, Kriging model)	9.5678^0	0.5876	8.2925	2.8120

5.4 Performance of the optimized wing

In this section, we measure the mean thrust force generated by the optimized wing – wing with $\theta = 9.567^0$, $\hat{r}_2 = 0.5876$ and AR = 8.2925 –at the different flapping frequency. The total weight of our flapper without control mechanism is around 8.3 g. With the addition of the control mechanism, the weight will be around 19 – 21 g. At 26.67 Hz of flapping frequency, our optimized wing produces

20.89 gf of thrust force. This thrust force is sufficient for the hover flight for our flapping wing micro air vehicle.

To demonstrate the flight capability of our FWMAV, we carried out the wired flight with stabilizer. The stabilizer is attached to the flapper as a substitute of the control mechanism. The total weight of the flapper with the stabilizer is 13.6 g. Figure 5.8 shows the hover flight of our FWMAV at a different period. The hover flight is recorded for more than 40 seconds. The sail shaped stabilizer reduced the undesirable moment, providing a favorable condition for the hover flight. Although the stabilizer provides a suitable condition for the hover flight, an appropriate control mechanism is required to manipulate the flapping flight.

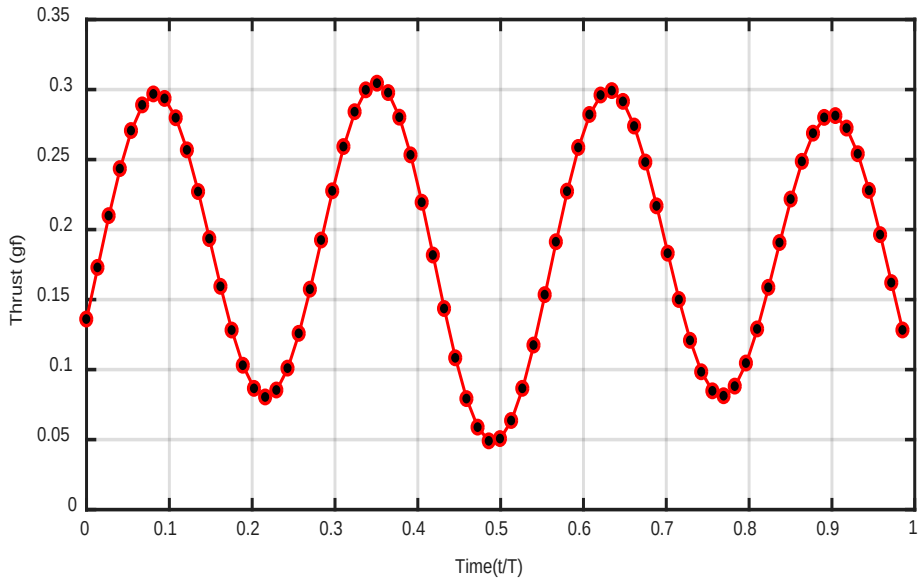

Figure 5. 5 Time history of the thrust generated by the optimized wing at 26.67 Hz

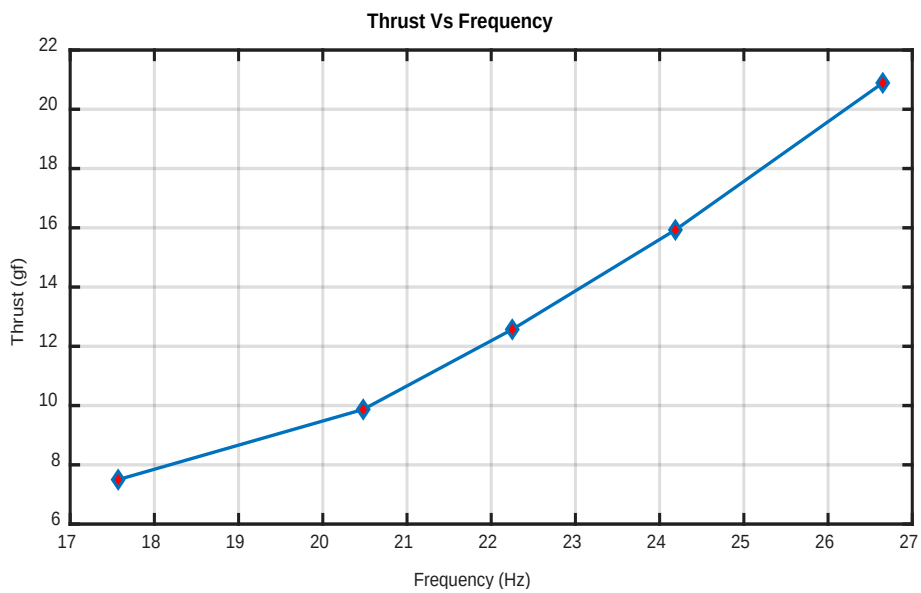

Figure 5. 6 Mean thrust generated by the optimized wing at different flapping frequency.

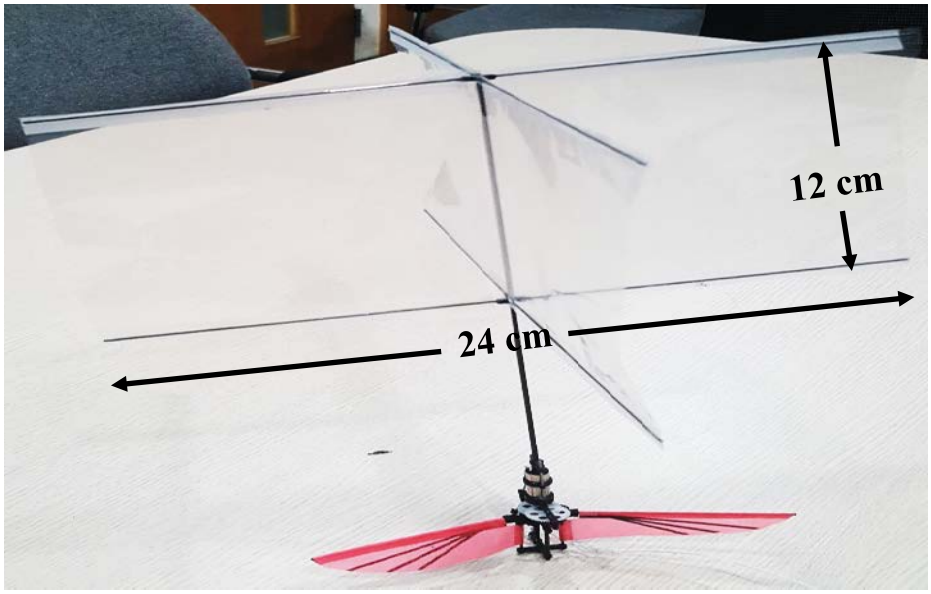

Figure 5. 7 Flapper with stabilizer

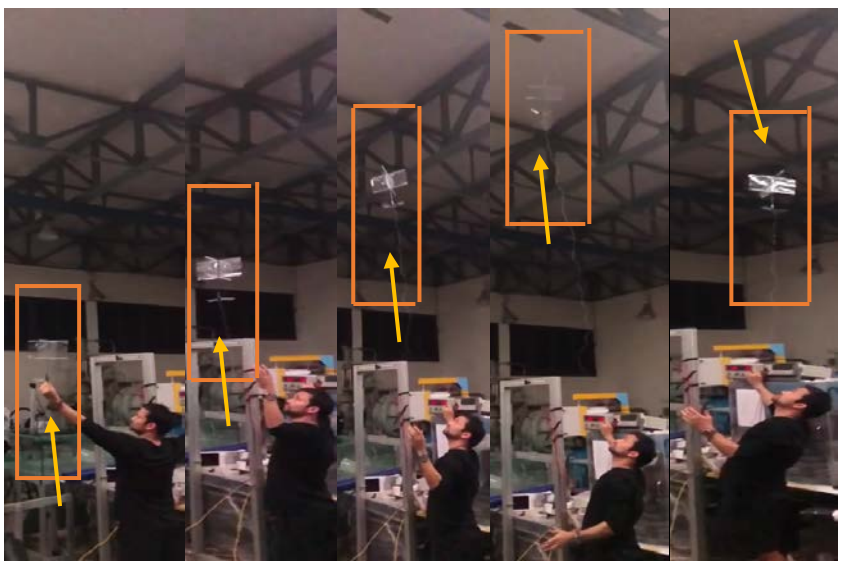

Figure 5. 8 Demonstration of FWMAV Lift off with a stabilizer

Chapter 6

Conclusions

In this research, the effect of wing geometric parameters like wing area, camber angle, non−dimensional radius of second moment of wing area and Aspect Ratio on the mean thrust generation and power efficiency is investigated using an iterative approach. Later on, an experimental design optimization is implemented with an objective of increasing the power efficiency of the flapping wing. A noisy Kriging model is constructed as the surrogate to consider the noise in the experimental data. EFI, an extended version of EI, is used to find the new points in the design space.

Wing geometric parameters like camber angle, non−dimensional radius of second moment of area and aspect ratio have a significant effect on the mean thrust generation and the power efficiency. With the increase of the camber angle, the power consumption decreases, while the mean thrust first rises, reaches the maximum and then plummets. Increasing the non−dimensional moment of wing area increase both the mean thrust and the power

efficiency. However, increasing the non-dimensional radius of second moment of wing area beyond 0.60 is not suggested as it reduces the root length of the wing, which may lead to structural failure of the wing. Furthermore, the highest power efficiency can be achieved when the Aspect Ratio of the flapping wing is around 8.

A surrogate based experimental design optimization is employed to optimize the flapping wing. We use EFI as an infill criterion, as it suggests a new point within the feasible region of the design space. Using this optimization process, we are able to enhance the power efficiency of the flapping wing. The best wing obtained from this optimization process is the wing with camber angle of 9.5678, non-dimensional radius of second moment of area of 0.5876 and aspect ratio of 8.2925.

Although we enhanced the wing performance by considering several wing geometric parameters, there are still many parameters that need to be considered to fully optimize the flapping wing. In this research, we use the fixed orientation of the wing vein for the entire wings. However, this position does not represent the optimum vein orientation. The wing performance is also influenced by the location and the thickness of the vein. Therefore, additional studies are needed on the wing veins to further improve the performance of the

flapping wing. Nevertheless, the present work provides the useful guidance for the design of the FWMAVs.

References

[1] T. Weis-Fogh, "Quick estimates of flight fitness in hovering animals," *J Exp Biol,* 1973.

[2] C. P. Ellington, C. Van Den Berg, and S. P. Sane, "Leading edge vortices in insect flight," *Nature,* 1996.

[3] J. M. Birch and M. H. Dickinson, "The influence of wing-wake interactions on the production of aerodynamic forces in flapping flight," *Journal of Experimental Biology,* vol. 206, no. 13, pp. 2257-2272, 2003.

[4] S. A. Ansari, K. Knowles, and R. Zbikowski, "Insectlike flapping wings in the hover part 1: effect of wing kinematics," *Journal of Aircraft,* vol. 45, no. 6, p. 1945, 2008.

[5] M. H. Dickinson, F.-O. Lehmann, and S. P. Sane, "Wing Rotation and the Aerodynamic Basis of Insect Flight," 1999.

[6] S. R. Jongerius and D. Lentink, "Structural Analysis of a Dragonfly Wing," *Experimental Mechanics,* vol. 50, no. 9, pp. 1323-1334, 2010.

[7] H. Ren, X. Wang, X. Li, and Y. Chen, "Effects of Dragonfly Wing Structure on the Dynamic Performances," *Journal of Bionic Engineering,* vol. 10, no. 1, pp. 28-38, 2013.

[8] J. W. Kruyt, G. F. van Heijst, D. L. Altshuler, and D. Lentink, "Power reduction and the radial limit of stall delay in revolving wings of different aspect ratio," *J R Soc Interface,* vol. 12, no. 105, Apr 6 2015.

[9] S. A. Ansari, K. Knowles, and R. Zbikowski, "Insectlike flapping wings in the hover part 2: effect of wing geometry," *Journal of Aircraft,* vol. 45, no. 6, p. 1976, 2008.

[10] N. Phillips, K. Knowles, and R. J. Bomphrey, "The effect of aspect ratio on the leading-edge vortex over an insect-like flapping wing," *Bioinspir Biomim,* vol. 10, no. 5, p. 056020, Oct 09 2015.

[11] G. Du and M. Sun, "Effects of wing deformation on aerodynamic forces in hovering hoverflies," *J Exp Biol,* vol. 213, no. Pt 13, pp. 2273-83, Jul 1 2010.

[12] S. M. Walker, A. L. Thomas, and G. K. Taylor, "Deformable wing kinematics in free-flying hoverflies," *J R Soc Interface,* vol. 7, no. 42, pp. 131-42, Jan 6 2010.

[13] Z. M. Fairuz *et al.*, "Effect of Wing Deformation on the Aerodynamic Performance of Flapping Wings: Fluid-Structure Interaction Approach," *Journal of Aerospace Engineering,* vol. 29, no. 4, p. 04016006, 2016.

[14] T. Q. Truong, V. H. Phan, H. C. Park, and J. H. Ko, "Effect of Wing Twisting on Aerodynamic Performance of Flapping Wing System," *AIAA Journal,* vol. 51, no. 7, pp. 1612-1620, 2013.

[15] J. Tommey and J. D. Eldredge, "Numerical and experimental investigation of the role of flexibility in flapping wing flight," *AIAA,* 2006.

[16] A. Gogulapati, P. P. Friedmann, and J. Martins, "Optimization of the Kinematics of a Flapping Wing MAV in Hover for Enhanced Performance," 2013.

[17] Y. Nan, M. Karasek, M. E. Lalami, and A. Preumont, "Experimental optimization of wing shape for a hummingbird-like flapping wing micro air vehicle," *Bioinspir Biomim,* vol. 12, no. 2, p. 026010, Mar 6 2017.

[18] A. Chaudhuri, R. T. Haftka, K. T. Chang, J. Van Hall, and P. Ifju, "Multi-Objective Experimental Optimization with Multiple Simultaneous Sampling for Flapping Wings," *AIAA,* 2015.

[19] F. Viana, R. Haftka, G. Venter, and R. Hamman, "Efficient Global Optimization with Experimental Data: Revisiting the Paper Helicopter Design," 2011.

[20] C. P. Ellington, "The aerodynamics of hovering flight . II Morphological parameters," 1983.

초록

정지비행시 날개짓 비행체의 날개형상에 대한 실험적 최적화 연구

곤충의 날개는 높은 기동력으로 정지 비행과 전진 비행을 할 수 있는 차세대 날갯짓 비행체인 초소형 날갯짓 비행체를(Flapping Wing Micro Air Vehicle) 개발하는데 있어 원천 요소 중 하나라고 볼 수 있다. FWMAV 의 효율적인 설계는 날개 형상의 파라메터에 대한 최적의 조합을 얻기 위해서 설계 공간에 대한 세밀한 분석이 필요하다. 본 연구는 정지 비행시 날갯짓하는 날개에 대한 성능을 높이기 위해 실험적 최적화 과정을 수행하였다.

자연에 있는 여러 곤충들의 날개는 서로 다른 값의 날개 형상 파라메터들의 조합으로 이루어져 있어 서로 다른 공기역학 성능을 가지고 있다. 다양한 날개의 파라메터 조합에 대한 효과를 이해하기 위해 먼저 몇몇 날개 형상에 대해 추력과 전력소모량을 반복 실험을 통하여 분석하였다. 그 결과 캠버각도, 무차원화된 이차면적모멘트, 가로세로비와 같은 날개 형상 파라메터가 추력과 효율에 큰 영향을 미친다는 것을 알 수 있었다. 다음은 최적화된 날개 형상을 얻기 위해 실험적 최적화를 수행하였다. 이때 실험에서 발생하는 노이즈를 고려하기위해 노이즈를 고려한 크리깅 모델을 사용하였다. 최적화 과정의 목표는 효율을 최대화하는 것이다. 디자인 결과

캠버각도 9.5678 도, 무차원화된 이차면적모멘트 0.5876, 가로세로비 8.2925 의 날개가 다른 형상의 날개보다 높은 효율을 가지는 것으로 나타났다. 날갯짓 주파수 26.67 Hz 에서 이 날개는 20.89g 의 추력을 보였다. 최적화된 날개의 비행 능력은 안정기를 장착한 비행시험으로 증명하였다.

학번: 2016-23334

Name: 디브야라즈

Acknowledgement

I would like to express my deepest gratitude to my advisor, Kim, Chongam, for providing me with this opportunity to carry out the research on the Flapping Wing Micro Air Vehicles (FWMAVs). I would like to thank Mr. Lee, Junhee for his advice and support, which made it possible to complete this work. I am also grateful to all my lab mates for academic support and friendship.

I would like to acknowledge the love and support of my family and friends. They kept me on track by providing motivations and showing confidence in my work.

I would like to thank everyone for letting me complete my thesis successfully.